Semiconductor Quantum Rods as Fluorescent Biological Labels

Aihua Fu[1], Weiwei Gu[2], Benjamin Boussert[1], Kristie Koski[1], Daniele Gerion[1], Liberato Manna[1], Mark Le Gros[3], Carolyn Larabell[2, 3] & A. Paul Alivisatos*[1,4]

[1]Department of Chemistry, University of California Berkeley, CA 94720

[2]Department of Anatomy, University of California San Franscisco, CA 94143

[3]Physical Biosciences Division, [4]Materials Sciences Division, Lawrence Berkeley National Laboratory, Berkeley, CA 94720

*Correspondence should be addressed to A. P. A. (alivis@berkeley.edu)

In recent years, semiconductor quantum dots have been applied with great advantage in a wide range of biological imaging applications [1-4]. The continuing developments in the synthesis of nanoscale materials and specifically in the area of colloidal semiconductor nanocrystals[5, 6] have created an opportunity to generate a next generation of biological labels with complementary or in some cases enhanced properties compared to colloidal quantum dots. In this paper, we report the development of rod shaped semiconductor nanocrystals (quantum rods) as new fluorescent biological labels. We have engineered biocompatible quantum rods by surface silanization and have applied them for non-specific cell tracking as well as specific cellular targeting. The properties of quantum rods as demonstrated here are enhanced sensitivity and greater resistance for degradation as compared to quantum dots. Quantum rods have many potential applications as biological labels in situations where their properties offer advantages over quantum dots.

The challenges of biological imaging demand further development of new molecular probes and contrast agents that have better sensitivity, longer stability, good biocompatibility and minimum invasiveness. The convergence of nanotechnology and biotechnology has created many innovations to meet this challenge. A variety of different approaches in making new nanoprobes have been developed in recent years. For example, nanoparticle-based bio-bar codes were reported for ultrasensitive detection of proteins[7]; Noble metal nanoparticles have been reported as molecular rulers based on plasmon coupling[8]; and magnetic nanocrystals have been shown as effective contrast agents for magnetic resonance imaging [9]. Among various nanomaterials developed, semiconductor nanocrystals, also known as quantum dots (QDs), represent one of the most successful new biological probes. Compared to conventional organic fluorophores, QDs have advantageous properties, including tunable emission, exceptional photostability, high multiplexing capability and extreme brightness [1-4]. QDs are now commercially available and used in an ever-widening array of biological applications.

The ability to manipulate the shape of semiconductor nanocrystals has led to rod shaped semiconductor nanocrystals, hereafter referred to as "quantum rods" (QRs) [5, 10, 11]. QRs are semiconductor nanocrystals with diameters ranging from 2 to 10nm and with lengths ranging from 5 to 100nm. The band gap of the rods depends strongly on diameter, but only weakly on length [12]. Thus emission can be readily tuned by diameter over the same spectral region as QDs, but the absorption cross section can be chosen using the length. In addition to the properties inherited from QDs, such as size-tunable broad absorption, narrow symmetric emission, and extreme resistance to photobleaching, QRs have many

unique properties that make them potentially better probes for some biomedical applications than QDs. For example, QRs have larger absorption cross section [13], faster radiative decay rate [14], bigger Stokes shift [5], and can be functionalized with multiple binding moieties. Furthermore, a single quantum rod exhibits linearly polarized emission unlike the plane-polarized light from a single quantum dot [5]. And the emission of single QRs can be reversibly switched on-off by external electric fields [15]. These unique properties make QRs highly desirable for certain biological applications and bring new possibilities for biological labeling. However, due to the large surface strain intrinsic to rod shaped particles [10], it is more challenging for surface modification of QRs in order to transfer them from organic solvents to physiological buffer conditions. Therefore, there is little work reported about using QRs for biomedical imaging and detection [16].

In this paper, we report the use of surface modified CdSe/CdS/ZnS core/shell QRs as a new generation of biological label, and demonstrate that QRs can be used in a variety of bio-imaging applications. QRs are longer than QDs, so for some applications they may prove too large. However, we found that they could be used in a surprisingly large number of situations. Further, for single molecule *in vivo* studies, they are much better than QDs.

Similar to QDs, high quality QRs as synthesized are only soluble in organic solvents. A variety of approaches have been used to render QDs or QRs water soluble and biocompatible. Silanization is one of the most powerful methods, as the resulting particles are truly biocompatible and extremely stable in biological environments. We

designed a robust coating method for surface silanization of core/shell QRs. To overcome the enhanced surface strain from a rod, silane molecules were added in the priming step under a condition that favored condensation (Fig. 1a), enabling a well-coated rod surface as compared to single-silane-molecule-priming as reported for the silanization of spherical QDs [17]. Moreover, most silanization steps were performed inside a sonicator with temperature control, promoting uniform coating and a highly reproducible process. The silanization procedure thus developed for QRs could be readily applied for making water-soluble QDs and other types of nanoparticles, representing a general method to modify surfaces of nanoparticles. QRs after silanization were stable in aqueous buffer for over 2 years. Fig. 1b shows the transmission electron microscopy (TEM) images of silanized QRs in neutral phosphate buffer (PB). The absorption and emission spectra of silanized QRs (Fig. 1c) show that the silanization process does not change the essential optical features of unsilanized QRs [10].

The silanized QRs are totally biocompatible. Previously our group demonstrated phagokinetic tracking with QDs [18, 19]. When live cells were cultured on a layer of silanized quantum dots, the cells ingested all the dots they passed over, leaving behind a particle free trail which correlates with the metastatic potential of different cell lines [19]. Similarly, various live cells could also incorporate silanized QRs as they migrate on a layer of the nanocrystals, without influence on cell division and migration (see Supplementary Fig. 1 online). The good biocompatibility of QRs was also evidenced by direct delivery with Chariot™ [20], a peptide non-covalently interacting with QRs and

transferring the cargo through the cell membrane (Fig. 1d). QRs showed no apparent adverse effect on cells over the time period (24 hours) of our experiment.

When properly encapsulated, colloidal QDs exhibit no adverse effects on cells over extended periods of time [19, 21, 22]. For instance, gene expression studies on human skin (HSF-42) and lung fibroblast (IMR-90) cells exposed to CdSe/ZnS nanocrystals with polyethylene glycol on the surface, showed no detectable change in gene expression profile over a period of days [22]. Likewise early stage *Xenopus* embryo development studies on lipid-coated CdSe/ZnS particles were normal [21]. Nonetheless, all CdSe/ZnS nanocrystals can eventually release Cadmium, and this rate of release can be varied depending upon the surface coating. We measured the Cd^{2+} leakage from both QRs and QDs by inductively coupled plasma optical emission spectroscopy (ICP/OES). Since ICP/OES measurements of Cd^{2+} concentration showed that same optical density (OD) of the nanocrystals at 488nm corresponds to same amount of CdSe material in a sample, we standardized the Cd^{2+} leakage from rod and dot samples by normalizing to the OD at 488nm of the original samples. For rod and dot samples that were silanized under the same condition and stored at 4ºC for 3 months, the Cd^{2+} concentration in the solution after nanocrystals being filtered was analyzed. Cd^{2+} present in filtered solution from the QR sample was less than one third of that filtered from the QD sample (Fig. 1e). This demonstrates that Cd^{2+} leakage was dramatically reduced by making the same amount of CdSe material into a rod shape versus that of a spherical shape. The decrease in Cd^{2+} leakage of QRs was partially due to the reduced ratio of the surface area over volume (See calculations in Supplementary Materials for particle geometries as shown in the

TEM images of Supplementary Fig. 2 online). The most important contribution to the reduction of quantum rod Cd^{2+} leakage arose from the reduced curvature effect in a rod shaped particle over that of a spherical particle, rendering the rod surface more resistant to such corrosion processes as photooxidation.

As mercapto, amino, carboxyl and phosphonate functional groups can be easily incorporated into the design of surface coating by silanization, silanized QRs can be conjugated with various biomolecules to achieve precise biological functions. Antibody-antigen affinity is one of the most specific biological interactions and widely used for fluorescence imaging. We tested the conjugation of silanized particles with mercapto surface groups to amino bearing antibodies through a cross linker sulfo-SMCC as schematized in Fig. 2a. Conjugation with either whole antibody IgG or antibody fragments were achieved and evidenced by delay of the mobility of conjugates in gel-electrophoresis. To compare the specific cellular labeling efficiency of QRs with QDs (both have a quantum yield of 9%), we picked a well-demonstrated system, that is, cancer cell marker Her2 on the surface of human breast cancer cell line SK-BR-3[23], for specific labeling tests. After incubating the cells with mouse anti-Her2 antibody that binds to the external domain of Her2, we added quantum rod-goat anti-mouse $F(ab')_2$ and quantum dot-goat anti-mouse $F(ab')_2$ conjugates with the same OD at 488nm. Specific targeting of the conjugates to cancer marker Her2 was clearly observed in both cases. Since the OD of QRs is the same as dots, the concentration of rods is only about 1/8 of that of dots. However under such condition, the detected staining signal from quantum rod conjugates is as bright as that from dot conjugates (Fig. 2c), which indicates that QRs are more

sensitive probes than QDs. This is expected because QRs have bigger absorption cross section than QDs at the same excitation wavelength [13]. At the same time, QRs are predicated to have faster radiative decay rates [14], which correspond to a increased number of excitation and emission cycles within a signal collection period.

Since increasing the number of labeling particles can also enhance the signal intensity for ensemble fluorescent labeling, the increased detection signal from QRs is advantageous but not exceptional in ensemble systems. The more attractive turnout from the brighter fluorescence of QRs is for single molecule fluorescent imaging. The ability to track single molecules is a powerful method to study the dynamic and kinetic behavior of biomolecules inside living cells. Although QDs were shown to be able to image single molecules in living cells [24, 25], the enhanced fluorescent signal from QRs makes them ideal probes for single molecule tracking. We compared the fluorescence signals of QRs and QDs at the single molecule level as evidenced by blinking. Under the same excitation and detection conditions, the fluorescent images of QRs were greatly improved from that of QDs (Fig. 3a, also see Movie 1a and 1b of supplementary material online). To quantitatively compare the fluorescent signals, both rod and dot images were analyzed by automatically collecting fluorescent signals from a 15-frame image sequence using a self-written Matlab program. Figure 3c shows the number of particles picked up through the program as a function of threshold intensity and threshold image number. Threshold intensity is the intensity value set to differentiate signal from background in the program, and threshold image number defines that a signal has to appear at least in a certain number of images to be picked up as a particle, which reflects the blinking property of

single particles, and also distinguishes particle from noise because noise tend to appear in only a small number of images. In the plot of QRs, with increasing threshold and threshold image number, the number of quantum rods holds basically an island of stability where there is a clean distinction between particles and noise. However, for quantum dots, the number of particles decreases very quickly and it is very difficult to distinguish between particles and noise. This is because as compared to QRs, QDs are not as bright so they are not statistically distinct from the noise and thus not quite as accurate a measurable quantity as the rods. To quantitatively compare the intensity of QRs and QDs, We extract the particle intensities at threshold intensity 10 and threshold image number 5 - one of the points in the island of stability of QRs. Histograms of intensity distribution of both QRs and QDs are plotted as inserts in Figure 3c. The mean intensity is 29.5 for QRs and 12.7 for QDs, proving QRs are much more intense fluorescent probes than QDs. It is worth noting that under this condition, only 883 QDs are selected compared to 1624 particles for QRs. So we are in fact comparing the intensities from the brighter portion of quantum dots with almost a whole body of QRs, which may contain some low emission rods with possibly defects or surface imperfections during growth [26]. Further improvements in synthesis giving an intensity ratio of rods to dots close to theoretical value of 8 should be possible and will show a more dramatic advantage for QRs in single molecule probing. Moreover, in Figure 3C the number of particles of QDs goes down much faster with increasing threshold image number than QRs, meaning QDs blink more or have longer off times than QRs. This is consistent with previous report that blinking arises because the dot radiative rate is slower

than a non-radiative mechanism [27]. Quantum rods have faster radiative decay rate [14], which may decrease the frequency of blinking thus yielding a better probe.

To demonstrate the ability of detecting and tracking of single QRs within living cells, we introduced small amount of silanized QRs to human breast cancer cell line MDA-MB-231 by the use of streptolysin-O (SLO), a bacterial protein that binds to cholesterol and forms holes in the plasma membrane of animal cells [28]. QRs retained their brightness inside living cells (Fig. 3c). The tracking at single molecule level was proved by particle blinking (see Movie 2 of the supplementary material online).

Although silanization only adds 2 or 3nm of coating thickness to nanocrystals (see supplementary Fig. 3 online), as rod sizes get bigger, they may interfere with the molecular events that they characterize, hence caution must be taken when time comes to interpret the data and a balance has to be found between the enhanced properties of QRs and the disadvantages in terms of their bigger sizes. However, this should not become an intrinsic limitation for single molecule tracking using QRs, as much bigger particles have been successfully applied in single molecule investigations [29].

The introduction of biocompatible semiconductor QDs in 1998 [30, 31] has led to tremendous advances in biotechnologically important applications, including multiplexed *in vivo* imaging[32, 33], long term single molecule tracking[24], deep tissue imaging and imaging guided surgery[34], as well as hybrid inorganic-bioreceptor based optical sensing [35]. In this paper, we have described the development of rod shaped semiconductor

nanocrystals for biological imaging. We have overcome the difficulty of rod surface modification and successfully transferred the nanocrystals from organic solvent to biological aqueous solutions by a silanization process. Silanized QRs have good biocompatibility and are potentially less cytotoxic than QDs. After further biofunctionization, QRs can be used as immunofluorescent probes. Compared to QDs, QRs are more intense and brighter probes, which is demonstrated clearly in single molecule imaging. The unique properties of QRs including distinctive shape, large absorption cross section, fast radiative decay rate, big stokes shift, multiple binding moieties, electric field induced switching of the fluorescence and linearly polarized emission have yet to be fully exploited. We anticipate biocompatible QRs with properties superior to organic fluorophores and spherical QDs will have a very beneficial impact in many aspects of biomedical imaging and detection schemes.

Acknowledgements

This work is supported in part by the DARPA/AFOSR DURINT Program Grant No. F49620-01-1-0474 under subcontract 066995 between the university of Southern California and the University of California Berkeley, and by the NIH National Center for Research Resources through the University of California subaward agreement 0980GFD623 through the U.S. Dept. of Energy under Contract No. DE-AC02-05CH11231, and by the Director, office of Energy Research, Office of Science, Division of Materials Sciences, of the U.S. Department of Energy under Contract No. DE-AC02-05CH11231. This work is also funded by the US Department of Energy, Office of Biological and Environmental Research (DE-AC02-05CH11231), the National Center for

Research Resources of the National Institutes of Health (P41 RR019664) and the National Institutes of General Medicine, NIH (GM070445).

Competing interests statement

The authors declare that they have no competing financial interests.

Methods

Materials. Dimethylcadmium ($Cd(CH_3)_2$, 97%) and tri-n-butylphosphine (TBP, 99%) were purchased from Strem. Selenium (Se, 99.999%), tri-n-octylphosphine oxide (TOPO, 99%), diethylzinc (1.0M solution in heptane), hexamethyldisilathiane ($(TMS)_2S$), tetramethylammonium hydroxide (TMAOH, pentahydrate 97%, or 25% (w/w) solution in methanol), (3-mercaptopropyl) trimethoxysilane (MPS, 95%), chlorotrimethylsilane (CTS, 99%) was purchased from Aldrich. Hexylphosphonic acid (HPA, 99%) was purchased from Organometallics Inc. Tetradecylphosphonic acid (TDPA, 98%) was purchased from Alfa. 2-[Methoxy(polyethylenoxy) propyl] trimethoxysilane (PEG-silane, 90%) was purchased from Gelest. Potassium phosphate (PB, monobasic or dibasic) was purchased from Sigma. UltraPure™ agarose was purchased from Invitrogen.

Synthesis of quantum rods. CdSe/CdS/ZnS QRs were synthesized following the published procedure [10]. All procedures were performed using standard air-free techniques. For CdSe core rods, 0.5g of $Cd(CH_3)_2$ in TBP (32.99% by weight) and 2.56g of Se in TBP (7.78% by weigth) were added to a mixture of 3.53g of TOPO, 0.3g TDPA and 0.08g HPA. Nanocrystals were growing at 300ºC for 7min. The sample was washed and dried under nitrogen, then stored in a glove box for shell growth with no further size selective precipitation. A CdS/ZnS gradient shell was grown by injecting 2ml of chloroform solution of CdSe rods with a concentration of 1g/L into 5g of TOPO. After pumping out all the chloroform, 0.5ml of CdS/ZnS stock solution from a mixture of 2.057g of TBP, 0.041g of $Cd(CH_3)_2$, 0.503g of diethylzinc and 0.078g of $(TMS)_2S$ was injected dropwise at 160ºC and reacted for 10min. The resulting CdSe/CdS/ZnS

core/shell rod solution was mixed with 3ml of octanol and stored in the dark inside glovebox.

Surface modification of quantum rods. A 1ml aliquot of CdSe/CdS/ZnS core/shell rods was precipitated using methanol, followed by addition of 200µl MPS. The sample was vortexed and then 1ml TMAOH was added. The resulting solution was sonicated at 65ºC for 2h. Afterwards, a dialysis solution of 450µl methanol and 1400µl of TMAOH was prepared, and 6ml of it was directly mixed with the former rods solution. The mixture was dialyzed for 1h, inside a Spectra/Por membrane (MWCO 25,000) tube (Spectrum Laboratories Inc). Next, 2µl MPS, 36µl H2O, 900µl PEG-silane was added and the sample was sonicated at 65ºC for 1.5h. The sample was then transferred into a 50ml flask under Ar_2. With vigorous stirring, 0.1ml CTS, 2ml methanol and 0.32g of solid TMAOH was added, followed by immediate heating of the sample to 60ºC for 30min. The sample was kept stirring at room temperature overnight, and concentrated with Microcon YM-100 filters. The concentrated sample was dialyzed in 1L of 10mM PB (pH 7.3) overnight. Afterwards, the sample was filtered through MILLEX®-GV 0.22µm filter unit (Millipore), and stored at 4ºC in a refridgerator.

Quantum rods or quantum dots antibody conjugation. 2mg of Sulfo-SMCC was added into 0.15ml of $F(ab')_2$ fragment (0.2mg) goat anti-mouse IgG (H+L) (Jackson ImmunoResearch), or whole goat anti-mouse IgG (H+L) (0.3mg) (Jackson ImmunoResearch), and reacted on a vortexer foam rack for 1h. The sample was then run through a NAP 5 column to remove unreacted sulfo-SMCC, with 50mM PB (pH 7.3) as

an elution buffer. Subsequently 51µl of QRs (OD 488nm 0.11753) or 20µl QDs (OD 488nm 0.30016) was mixed with 260µl of sulfo-SMCC labeled antibody and 49µl 1M NaCl. Then, 31µl 10mM PB (pH 7.3) was added into the dot- antibody solution to render the solution volume the same as that of rod-antibody solution. Conjugating reaction solution was left on a vortexer foam rack for 2h at room temperature. Next, conjugates were washed using Microcon YM-100 filter. Afterwards, an aliquot of conjugates were analyzed by 3% agarose gel electrophoresis under a voltage of 10 V/cm (Bio-Rad). The remainder of conjugates was stored at 4ºC in a refrigerator overnight before immunolabeling.

Quantum rods characterizations. Optical absorbance was measured on an HP-8453 UV-Vis spectrophotometer (Hewlett-Packard). Fluoresence was measured using a SPEX Fluorolog-3 spectrofluorometer (Jobin Yvon horiba). TEM was measured on a FEI TECNAI G^2 microscope under 200 keV. Cd^{2+} concentration was analyzed on a Perkin Elmer 5300 DV Optical Emission ICP.

Cell culture. MDA-MB-231 and SK-BR-3 cells were obtained from ATCC. Cells were cultured in the appropriate media as following: MDA-MB-231 cells in Leibovitz's L-15 (ATCC) supplemented with 10% fetal bovine serum (Gibco); SK-BR-3 cells in McCoy's 5A medium (ATCC) plus 10% fetal bovine serum.

Cellular uptake of nanocrystals. For Chariot™ [20] mediated QRs uptake, the cells were subcultured in 8-well chambered cover glass slides (LabTEK) pre-coated with collagen

(Vitrogen) at a density of 10,000 cells per well. 80ng/ml Chariot and 2nM silanized QRs (in PBS) were incubated at room temperature for 30 min. Cell medium was aspirated. Immediately after washing the cells with warm PBS, 50 μL of Chariot-QRs mixture was added to each well, followed by 100 μL serum free medium. The cells were incubated at 37°C in the tissue culture incubator for 1h and then 250 μL of medium supplemented with 16% serum was added to each well. The cells were either imaged right away or left in the incubator for later observation. For Streptolysin O (SLO, sigma) mediated quantum rod uptake, the procedure was modified according to literature [28]. In general, cells were trypsinized and washed twice with serum free medium. About 4 millions cells were then incubated with 0.5nM QRs and 40U/ml SLO at 37°C for 20 min. The transfection was stopped by adding complete growth medium and incubated for another 20 min. Cells were washed in complete growth medium twice and put on cover glass for imaging, or sub-cultured in 8-well chambered cover glass slides for later observation.

Immunofluorescence labeling. Cells were fixed in 4% paraformaldehyde (Ted Pella) in cytoskeleton buffer (CSK: 100 mM KCl, 3 mM $MgCl_2$, 5 mM PIPES, 150 mM sucrose, pH 6.8) at room temperature for 30 min. Cells were rinsed in Superblock (SB, Pierce) (5 min x 3), then incubated in a solution of 1:100 anti-human, 1:100 anti-mouse Fab fragments (Jackson ImmunoResearch), and 10% goat serum (GS, Gibco), in SB for 30 minutes to block non-specific labeling. After rinsing, cells were incubated in mouse anti-Her2 antibody (1:30, zymed) in SB + 10% GS for 1h while rocking at room temperature. They were washed (5 min x 3) with phosphate buffer saline (PBS) and incubated in goat anti-mouse conjugated QRs or dots (OD 0.0613 at 488nm with 0.2cm pass length) in PBS

for 1h, and then washed again (5 min x 3) in PBS and ready to be observed. Control cells were treated with primary antibody ani-Her2, however for the secondary antibody-labeling step, unconjugated quantum rods/dots were added.

Fluorescence microscopy. A Zeiss AxioVert 200M fluorescence inverted microscope with a 103-watt mercury lamp and an AxioCam MRm CCD camera was used. Fluorescence signal was detected using either a Cy3.5 filter set (zeiss, exciter: BP 565/30, emitter: BP 620/60) or a QDot 605 filter set (chroma, exciter: E460SPUV, emitter: D655/20m). For detection of single molecules, 2 μL of 0.6 nM QRs, or 2 μL of 5 nM QDs were deposited on cover glass, dried using a compressed air blower, and then imaged with the microscope using a 60X 1.4 NA oil immersion lens. For detection of single molecules inside the cells, the MDA-MB-231 cells were first loaded with small amounts of QRs with the use of SLO (see above part of cellular uptake of nanocrystals), and imaged with a 60X 1.4 NA oil immersion lens. For other fluorescence microscope experiments, a 40X 1.2 NA water immersion lens were used.

Statistical analysis. A Matlab program was written to analyze single particle fluorescence images. First, all images were averaged into a single image and the particle positions were determined by selecting the brightest pixels in the conjoined image. Further, the most intense pixels corresponding to single particle fluorescence are selected by three criteria: (i) an average minimum distance between bright pixels, (ii) an average minimum intensity, (iii) a minimum number of images that the bright pixel appears in. The average minimum threshold distance was chosen to be five pixels. This criteria was

chosen based on the conjoined image and the pixel distance necessary to distinguish between single particles and to select only a single pixel if there appeared to be a cluster of bright pixels. The average minimum intensity is a threshold intensity that is greater than that of the background such that only pixels distinguishable from the background are selected. In addition, since single particles blink and noise will appear in only a small number of images, a threshold image number is used to reflect the blinking property of single particles and to distinguish noise from particles. The intensities of each particle are then tracked in each subsequent image. With a threshold distance set to five, a threshold image number of five, and a threshold intensity of ten, 883 particles were found in the QD images with a mean intensity of 12.7 and 1624 particles were found in the QR images with a mean intensity of 29.5.

References:

1. Medintz, I.L., Uyeda, H. T., Goldman, E. R., and Mattoussi, H Quantum dot bioconjugates for imaging, labelling and sensing. *Nature Materials* **4**, 435-446 (2005).

2. Alivisatos, A.P., Gu, W. & Larabell, C. Quantum dots as cellular probes. *Ann. Rev. Biomed. Eng.* **7**, 55-76 (2005).

3. Fu, A., Gu, W., Larabell, C. & Alivisatos, A.P. Semiconductor nanocrystas for biological imaging. *Current Opinion in Neurobiology* **15**, 568-575 (2005).

4. Michalet, X., Pinaud, F. F., et. al. Quantum Dots for live cells, in vivo imaging, and diagnostics. *Science* **307**, 538-544 (2005).

5. Hu, J.T. et al. Linearly polarized emission from colloidal semiconductor quantum rods. *Science* **292**, 2060-2063 (2001).

6. Manna, L., Milliron, J. D., Meisel, A., Scher E. C., Alivisatos, A. P. Controlled growth of tetrapod-branched inorganic nanocrystals. *Nature Materials* **2**, 382-385 (2003).

7. Nam, J., Thaxton, C. S., Mirkin, C. A. Nanoparticle-based bio-bar codes for the ultrasensitive detection of proteins. *Science* **301**, 1884-1886 (2003).

8. Sonnichsen, C., Reinhard, B. M., Liphardt, J., Alivisatos, A. P. A molecular ruler based on plasmon coupling of single gold and silver nanoparticles. *Nature Biotechnology* **23**, 741-745 (2005).

9. J.L. Turner et al. Synthesis of Gadolinium-Labeled Shell-Crosslinked Nanoparticles for Magnetic Resonance Imaging Applications. *Advanced Functional Materials* **15**, 1248-1254 (2005).

10. Manna, L., Scher, E.C., Li, L.S. & Alivisatos, A.P. Epitaxial growth and photochemical annealing of graded CdS/ZnS shells on colloidal CdSe nanorods. *Journal Of The American Chemical Society* **124**, 7136-7145 (2002).

11. Peng, X., Manna, L., Yang, W., Wickham, J., Scher, E., Kadavanich, A., Alivisatos, A. P. Shape control of CdSe nanocrystals. *Nature* **404**, 59-61 (2000).

12. Li, L.S., Hu, J.T., Yang, W.D. & Alivisatos, A.P. Band gap variation of size- and shape-controlled colloidal CdSe quantum rods. *Nano Letters* **1**, 349-351 (2001).

13. Htoon, H., Hollingworth, J. A., Malko, A. V., Dickerson, R., Klimov, V. I. Light amplification in semiconductor nanocrystals: Quantum rods versus quantum dots. *Applied Physics Letters* **82**, 4776-4778 (2003).

14. Shabaev, A., Efros, L. 1D Exciton Spectroscopy of Semiconductor Nanorods. *Nano Lett.* **4**, 1821-1825 (2004).

15. Rothenberg, E., Kazes, M., Shaviv, E., Banin, U. Electric field induced switching of the fluorescence of single semiconductor quantum rods. *Nano Lett.* **5**, 1581-1586 (2005).

16. Tsay, M.M., Doose, S., Weiss, S. Rotational and translational diffusion of peptide-coated CdSe/CdS/ZnS nanorods studied by fluorescence correlation spectroscopy. *J. Am. Chem. Soc.* **128**, 1639-1647 (2006).

17. Gerion, D., Pinaud, F., Williams, S. C., Parak, W. J., Zanchet, D., Weiss, S., Alivisatos, A. P. Synthesis and Properties of Biocompatible Water-Soluble Silica-Coated CdSe/ZnS Semiconductor Quantum Dots. *J. Phys. Chem. B* **105**, 8861-8871 (2001).

18. Parak, W.J. et al. Cell motility and metastatic potential studies based on quantum dot imaging of phagokinetic tracks. *Advanced Materials* **14**, 882-885 (2002).

19. Pellegrino, T. et al. Quantum dot-based cell motility assay. *Differentiation* **71**, 542-548 (2003).

20. Morris, M.C., Depollier, J., Mery, J., Heitz, F. & Divita, G. A peptide carrier for the delivery of biologically active proteins into mammalian cells. *Nature Biotechnology* **19**, 1173-1176 (2001).

21. Dubertret, B., Skourides, P., Norris, D.J., Noireaux, V., Brivanlou, A. H., Libchaber, A. In Vivo imaging of quantum dots encapsulated in phospholipid micelles. *Science* **298**, 1759-1762 (2002).

22. Zhang, T., Stilwell, J. L., Gerion, D., Ding, L., Elboudwarej, O., Cooke, P. A., Gray, J. W., Alivisatos, A. P., Chen, F. F. Cellular Effect of High Doses of Silica-Coated Quantum Dot Profiled with High Throughput Gene Expression Analysis and High Content Cellomics Measurements. *Nano. Lett.* **6**, 800-808 (2006).

23. Wu, X., Liu, H., Liu, J., Haley, K. N., Joseph, A. T., Larson, J. P., Ge, N., Peale, F., Bruchez, M. P. Immunofluorescent labeling of cancer marker Her2 and other cellular targets with semiconductor quantum dots. *Natuer Biotechnology* **21**, 41-46 (2003).

24. Dahan, M. et al. Diffusion dynamics of glycine receptors revealed by single-quantum dot tracking. *Science* **302**, 442-445 (2003).

25. Lidke, D.S. et al. Quantum dot ligands provide new insights into erbB/HER receptor-mediated signal transduction. *Nature Biotechnology* **22**, 198-203 (2004).

26. Ebenstein Y., M.T., Banin U. Fluorescence quantum yield of CdSe/ZnS nanocrystals investigated by correlated atomic-force and single-particle fluorescence microscopy. *Applied Physics Letters* **80**, 4033-4035 (2002).

27. Nirmal, M., Dabbousi, B. O., Basendi, M. G., Macklin, J. J., Trautman, J. K., Harris, T. D., Brus, L. E. Fluorescence intermittency in single cadmium selenide nanocrystals. *Nature* **383**, 802-804 (1996).

28. Giles, R.V., Grzybowski, J., Spiller, D.G. & Tidd, D.M. Enhanced antisense effects resulting from an improved streptolysin-O protocol for oligodeoxynucleotide delivery into human leukaemia cells. *Nucleosides & Nucleotides* **16**, 1155-1163 (1997).

29. Itoh, H., Takahashi, A., Adachi, K., Noji, H., Yasuda, R., Yoshida, M., Kinosita K. Jr Mechanically driven ATP synthesis by F1-ATPase. *Nature* **427**, 465-468 (2004).

30. Bruchez, M.J., Maronne, M., Gin, P., Weiss, S., Alivisatos, A. P. Semiconductor nanocrystals as fluorescent biological labels. *Science* **281**, 2013-2016 (1998).

31. Chan, W.C.W., Nie, S. Quantum dot bioconjugates for ultrasensitive nonisotopic detection. *Science* **281**, 2016-2018 (1998).

32. Gao, X., Cui, Y., Levenson, R. M., Chung, L. WK., Nie, S. In Vivo cancer targeting and imaging with semiconductor quanutm dots. *Nature Biotechnology* **22**, 969-976 (2004).

33. Stroh, M., Zimmer, J. P., et. al. Quantum dots spectrally distinguish multiple species within the tumor milieu in vivo. *Nature Medicine* **11**, 678-682 (2005).

34. Kim, S., Lim, YT., Soltesz, EG., De Grand, AM., Lee, J., Nakayama, A., Parker, JA., Mihaljevic, T., Laurence, RG., Dor, DM., et. al. Near-infrared fluorescent type II quantum dots for sentinel lymph node mapping. *Nature Biotechnology* **22**, 93-97 (2004).

35. Medintz, I.L., Clapp, A. R., Mattoussi, H., Goldman, E. R., Fisher, B., Mauro, J. M. Self-assembled nanoscale biosensors based on quantum dot FRET donors. *Nature Materials* **2**, 630-638 (2003).

Figure Legends

Figure 1. (a) A cartoon illustrating silanization of quantum rods. Crosslinked silanes are priming molecules for the surface coating. (b) TEM image of silanized rods in neutral phosphate buffer. Scale bar = 100 nm. (c) The UV-Vis absorption and emission spectra of silanized rods. The blue curve is the absorption spectrum; the red curve is the emission spectrum. (d) Silanized rods are biocompatible and non-toxic to living cells. The red fluorescence in the images is from quantum rods in human breasts cancer cells MDA-MB-231 after 1h (left) and 24h (right) transfected with Chariot™. These are merged images of transmission and fluorescent micrograms. Scale bar is 20 μm. (e) Rod shaped nanocrystals reduce the Cd^{2+} leakage significantly over that of spherical nanocrystals. The Cd^{2+} leakage was assayed by ICP/OES.

Figure 2. (a) Scheme for antibody bioconjugation of quantum rods. (b) Electrophoresis analyses of quantum rods/dots bioconjugation. Top, quantum rods/dots conjugated with $F(ab')_2$ fragment of goat anti-mouse IgG antibody. Bottom, quantum rods/dots conjugated with whole goat anti-mouse IgG antibody. The conjugates moved slower than the free nanocrystals (control) due to the linkage with antibodies. (c) Immunofluorescence labeling of breast cancer cell marker Her2 on breast cancer cells SK-BR-3. The Her2 marker was labeled with mouse anti-Her2 antibody and goat anti-mouse IgG $F(ab')_2$ conjugated quantum rods/dots. The bottom images show that there is minimum binding of free nanocrystals to the anti-Her2 antibody treated cells. Scale bar is 20 μm.

Figure 3. Fluorescence microscope images show that at the single molecule level, quantum rods (a) are much brighter than quantum dots (b). (c) Statistical results of rods (top) and dots (bottom) from 15 image sequences. The color plots are the natural logarithm of number of particles at different threshold intensity and threshold image number (the number of images that one particle at least appears in the 15 image sequence, for example, using a threshold image number 5 selects all the particle appears in at least 5 images of the 15 image sequence.) The Ln(Number of Particles) plots clearly illustrate how hard it is to differentiate particles from background noise for QDs, as one can see that the particle number decreased all the way down dramatically when the threshold and threshold image number are increased. However, for the rod case, there is a broad region where the number of rod particles is relatively the same with increasing threshold and threshold image number. The inserts are the histograms of particle intensity distribution when using threshold 10, and threshold image number 5, which pick up 1624 rods giving a mean intensity of 29.5, and pick up 883 dots with a mean intensity of 12.7. Please note the much smaller number of particles picked up for QDs. In another word, only bright dot particles with relatively long on time of dots are considered in the statistics. (d) Single rods (indicated by arrows) are still very bright inside live MDA-MB-231 human breast cancer cells. Scale bar is 10 μm.

Figure 1.

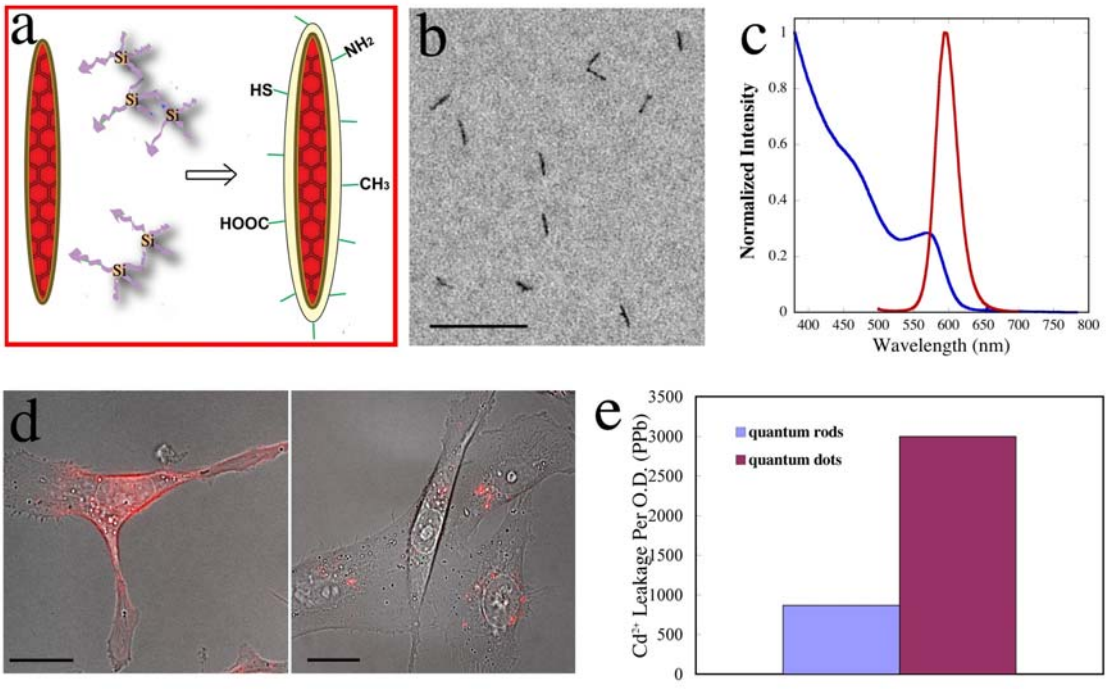
a
Si
Si
Si
Si
Si
HS
NH2
CH3
HOOC
b
c
Normalized Intensity
0
0.2
0.4
0.6
0.8
1
400 450 500 550 600 650 700 750 800
Wavelength (nm)
d
e
Cd2+ Leakage Per O.D. (PPb)
0
500
1000
1500
2000
2500
3000
3500
quantum rods
quantum dots

Figure 2.

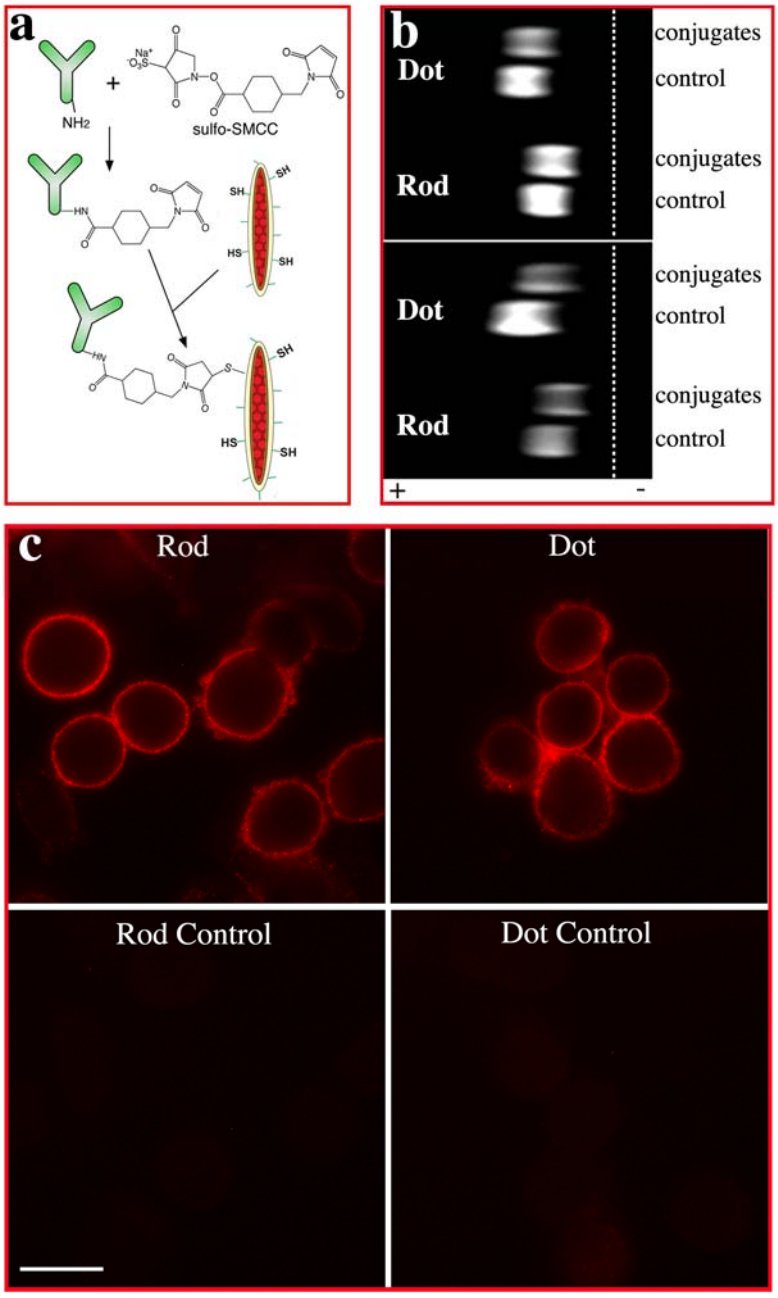
a
NH2
sulfo-SMCC
SH
HS
b
Dot
Rod
Dot
Rod
conjugates
control
conjugates
control
conjugates
control
conjugates
control
+
-
c
Rod
Dot
Rod Control
Dot Control

Figure 3.

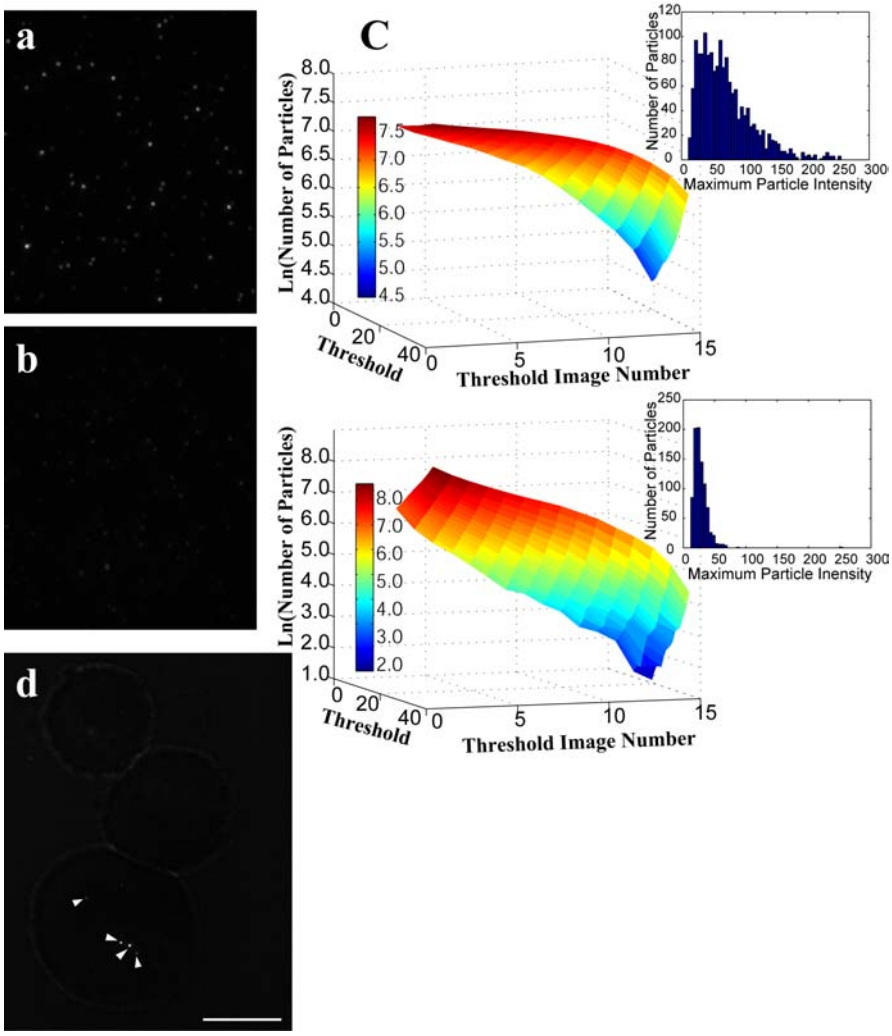
a
b
d
C
Ln(Number of Particles)
Threshold
Threshold Image Number
Number of Particles
Maximum Particle Intensity
Ln(Number of Particles)
Threshold
Threshold Image Number
Number of Particles
Maximum Particle Inensity